



Microtubule patterning in the presence of moving motor proteins



D. White^{a,*}, G.de Vries^b, J. Martin^b, A. Dawes^c

^a Li Ka Sheng Institute of Virology, University of Alberta, Edmonton, AB, Canada

^b Mathematical and Statistical Sciences, University of Alberta, Edmonton, AB, Canada

^c Department of Molecular Genetics, Ohio State University, Columbus, OH, USA

HIGHLIGHTS

- We model the dynamic interactions between microtubules and motor proteins.
- We describe microtubule patterns that can be formed in the presence of motors.
- For single motor types, we show that asters and vortices can form.
- For two opposing motors, we find that anti-parallel microtubule bundles form.

ARTICLE INFO

Article history:

Received 20 June 2014

Received in revised form

31 October 2014

Accepted 24 June 2015

Available online 6 July 2015

Keywords:

Microtubule

Motor protein

Patterning

Partial differential equations

ABSTRACT

Cytoskeletal polymers such as microtubules (MTs) interact with motor proteins to form higher-order structures. *In vitro* experiments have shown that MT patterns such as asters, bundles, and vortices can form under the influence of a single type of dynamic motor protein. MTs also can form anti-parallel bundles, similar to bundles that form the mitotic spindle during cell division, under the influence of two types of moving motors with opposite directionality. Despite the importance of MT structures, their mechanism of formation is not yet understood. We develop an integro-partial differential equation model to describe the dynamic interactions between MTs and moving motor proteins. Our model takes into account motor protein speed, processivity, density, and directionality, as well as MT treadmilling and reorganization due to interactions with motors. Simulation results show that plus-end directed motor proteins can form vortex patterns at low motor density, while minus-end directed motor proteins form aster patterns at similar densities. Also, motor proteins with opposite directionality are able to organize MTs into anti-parallel bundles. Our model is able to provide a quantitative and qualitative description of MT patterning, providing insights into possible mechanisms of spindle formation.

© 2015 Elsevier Ltd. All rights reserved.

1. Introduction

Microtubules (MTs) and motor proteins interact *in vivo* and *in vitro* to form a variety of patterns. *In vivo*, the organization of MTs is directly connected to the cellular process that a cell is carrying out (Dogterom and Surrey, 2013), such as cell division, cell motility, and cell polarization (Karp, 1996). For example, during cell division, MTs form two asters (as in Fig. 1 (a)) at the spindle poles of the cell, that are separated by an anti-parallel bundle of MTs (as in Fig. 1(b)). It should be noted that for these processes to be carried out, it is not only motor proteins that contribute to moving MTs into their proper organizations, but also many other cellular components and proteins. For example, the motor protein dynein attaches itself to the surface (with the aid of

other cellular proteins), and it is thought to help in creating the pushing and pulling forces on MTs that are required to properly align the MT asters at the cell's poles during cell division (Ma et al., 2014). *In vitro*, experiments show that in systems comprised solely of MTs and motor proteins (Nedélec et al., 1997; Surrey et al., 2001; Nedélec and Surrey, 2001), MTs can organize into asters, vortices, and bundles, as shown in Fig. 1. Here, we develop a mathematical framework to describe the interactions between moving motors and MTs. Our goal is to describe the patterns found *in vitro*, and to gain insight into how motors contribute to MT patterning *in vivo*.

Previously, partial differential equation (PDE) models have been developed to describe MT patterning in MT/motor systems (Aranson and Tsimring, 2006; Jia et al., 2008; Kim et al., 2003; Lee and Kardar, 2001). Such models have been successful at describing some of the MT patterns found *in vitro* by incorporating many of the important mechanisms required for MT patterning. Some of these mechanisms include motor density, speed, directionality, processivity, as well as MT reorientation, caused by interactions

* Corresponding author.

E-mail address: dtwhite@ualberta.ca (D. White).

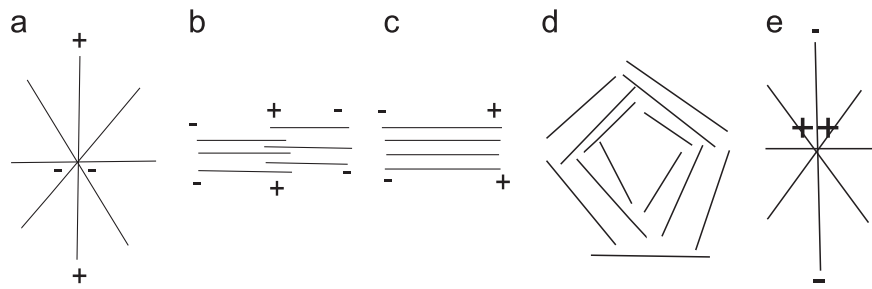


Fig. 1. Examples of MT organization *in vivo* and *in vitro*. *In vivo* organizations include (a) an aster with minus ends at the center (typical of a centrosomal configuration found in non-dividing cells and moving cells), (b) an anti-parallel bundle (similar to the mitotic spindle of a typical dividing cell), and (c) parallel bundles (similar to those found along the axon of a neuron). *In vitro* examples of MT patterns formed in systems comprised of only MTs and motor proteins include those described in (a), (b), and (c), but also include (d) vortices, and (e) an aster with plus ends at the center (Nedélec et al., 1997; Surrey et al., 2001).

with motor proteins. Here, we expand this list of mechanisms to include MT treadmilling, motor activity (the cross-linking capability of a motor), as well as the effect of two opposing motor types.

MTs are dynamic protein polymers formed through the self-assembly of α -, β -tubulin dimers (Karp, 1996; Wade, 2009). They grow through the addition of GTP-bound tubulin dimers, generally from the plus end of the MT, and shrink through dissociation of GDP-bound tubulin at this end. The minus end of the MT is generally more stable, being capped by stabilizing proteins. Two primary types of dynamic movement that MTs undergo are treadmilling (Waterman-Storer and Salmon, 1997; Mitchison and Kirschner, 1986) and dynamic instability (Waterman-Storer and Salmon, 1997; Kirschner and Mitchison, 1984). MT treadmilling is a chemical process that is defined as the steady-state, unidirectional flux of subunits through a polymer, as a result of continuous net assembly at one end of a polymer and continuous net disassembly at the other end. This type of dynamics results in the directed (constant) motion of the MT towards its plus end. Treadmilling has been observed *in vivo*, but can be difficult to reproduce *in vitro*. Dynamic instability refers to slow growth of a MT at its plus end, followed by fast depolymerization and has been observed both *in vivo* and *in vitro*.

Motor proteins are ATPases, and so are driven by the hydrolysis of adenosine triphosphate (ATP) (Howard, 2001). By transforming chemical energy into work, they are able to perform a number of important functions such as walking along MTs (either towards their plus end or minus end) and transporting molecular cargo across the cell. Motor proteins affect MT organization by cross-linking adjacent MTs (Nedélec et al., 1997). As motors walk along the cross-linked MTs, they produce pushing and pulling forces that help to reorient the MTs. Motor proteins can also slide MTs. MT sliding occurs when a motor is attached (absorbed) to a non-moving substrate at its cargo domain, where its free legs are able to attach to a MT (Yokota et al., 1995; Gibbons et al., 2001). Since the motor remains stationary, it effectively pushes the MT along its own axis as it walks along it. Sliding has been replicated in *in vitro* experiments (called gliding assays) (Yokota et al., 1995; Gibbons et al., 2001; Tao et al., 2006; Vale et al., 1992) and has been studied mathematically by White et al. (2014), as well as by Aranson and Tsimring (2006) and Aranson and Tsimring (2006). For the model developed and studied here, we do not consider MT sliding. However, translocation of MTs by sliding is shown to be an important mechanism for pattern formation, and is explained briefly in the discussion section of the paper.

The particular properties of motor proteins, such as their speed, directionality, and processivity, as well as their concentrations, determine what types of MT patterns can form. Some motors, such as kinesin-14, are fast (0.1 $\mu\text{m/s}$) and walk towards the minus end of a MT (and are called minus-end directed), while other motors, like kinesin-5, are very slow (0.04 $\mu\text{m/s}$), and walk towards the

plus end of a MT (and are called plus-end directed). MT processivity refers to the length of time a motor protein attaches to and walks along a MT (without detaching from the MT). Some motors, like kinesin-1 (conventional kinesin), can attach to MTs and walk long distances along them (processive), while others, like kinesin-5, can only walk short distances along MTs before detaching from them (weakly processive motors). Some motors, like kinesin-14, can attach to MTs but cannot walk along them for any significant amount of time (non-processive).

For MTs, both local and non-local models have been proposed to describe how MTs evolve in the presence of motor proteins. Defining a model as local or non-local refers to the treatment of the redistribution part of the model; in our case, this corresponds to MT reorientation (governed by motor proteins). Most models of MT evolution describe MT reorientation using local diffusion-type terms (Jia et al., 2008; Kim et al., 2003; Lee and Kardar, 2001). For example, the model of Lee and Kardar (2001) suggests that MTs undergo small reorientations in the presence of motor proteins. However, we know from recent *in vitro* studies that large reorientations are possible (Nedélec et al., 1997; Nedélec and Surrey, 2001). Thus, models that use integral terms to describe MT angular redistribution, that is, non-local models, are more reasonable from a biological perspective. Non-local models describe redistribution in terms of probabilities, and are referred to as velocity-jump models (Othmer, 2010). Such models have a rich history in the study of large-scale animal movement governed by certain cues that can exist over large distances (Othmer et al., 1988). More recently, such models have been used to describe the evolution of cellular systems (Hillen, 2006). A recent example of such a non-local model used in MT/motor systems is a study by Aranson and Tsimring (2006). This model uses a diffusion term to describe small scale fluctuations of MTs in the absence of motors, and also includes a non-local term to describe alignment of MTs as they collide with one another. The action of the motor proteins is implicit (Aranson and Tsimring, 2006), and suggests that motors are dispersed uniformly throughout space, so that when two MTs interact, they instantaneously align due to motor protein action. A second example of a non-local MT/motor model is that by White et al. (2014), in which MT patterning is examined using a similar integral term as in Aranson and Tsimring (2006) to describe MT redistribution. However, in White et al. (2014), the probability of alignment is based on more complex interactions between MTs and motors. In particular, the probability of alignment depends on the mean MT orientation, as well as the motor density and motor activity. Also in the model of White et al., MT patterning occurs under the influence of stationary motor proteins, as opposed to moving motors. In this paper, we extend the model of White et al. (2014) to take into account the mobility of motors.

To model motor protein dynamics, it is attractive to use a single advection-diffusion equation to account for the combined

dynamics of directed transport of motors along MTs, and diffusion of motors in the absence of MTs (Aranson and Tsimring, 2006; Lee and Kardar, 2001). However, such a model does not describe the two possible states that motors can be in: bound or unbound. Similar to Kim et al. (2003), we therefore separate the dynamics of motors into two equations, one for bound motors and the other for unbound, where an advection equation is used for bound motors and a diffusion equation is used for unbound motors. The combined advection–diffusion system has switching terms, to describe the rate at which bound motors detach from MTs (and become unbound motors), and the rate at which unbound motors attach to MTs (and become bound motors). Such a system of equations is more biologically realistic than a single reaction–diffusion equation, because it includes the switching rates between bound and unbound motors. These rates describe motor processivity and, as we will see in Section 3, varying such rates can change the qualitative MT patterns that are observed in simulations.

To summarize, our model consists of a non-local transport equation to describe the combined dynamics of MT directed transport by treadmilling and MT reorientation by motors, and a pair of equations (an advection–reaction equation and a diffusion–reaction equation) to describe the dynamics of bound and unbound motors. Our model for MT movement is non-local because it describes large scale reorientations of MTs using an integral-type term. In particular, MTs can make large reorientations in the presence of motor proteins, with particular orientations more likely than others. We define the probability of realignment, and the rate of realignment, in terms of biological observations of interactions between MTs and motors. In particular, for the probability of MT realignment, we include a description for how well motors can cross-link MTs (motor activity). Also, we define a motor density dependent realignment rate. To describe MT treadmilling, we include an advection term for MTs. At the microscopic scale, treadmilling involves the addition and subtraction of tubulin units at opposite ends of the MTs (as explained in Introduction). However, we do not model this small scale behavior, but rather assume that the overall dynamics result in the directed transport of a MT along its axis in the direction at which tubulin dimers are added (towards the plus end). Such a description has been used previously for modeling the dynamics of MTs in fish melanophore cells (Cytrynbaum et al., 2006). Here, for mathematical simplicity (Hillen et al., 2015), we consider only treadmilling (and not dynamic instability), so MTs are fixed length.

In Section 2 of this paper, we outline our modeling process, and in Section 3, we describe the simulation results. In Section 3.1, we describe the results of simulations using one motor type, and we show that low densities of plus-end directed motors organize MTs into vortices. At similar motor density, minus-end directed motors organize MTs into aster patterns. Also, we expand our model to include two motor types (motors with opposite directionality) by

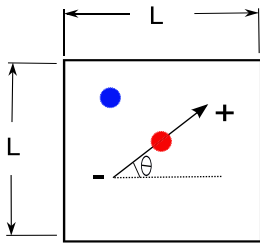


Fig. 2. Schematic of microtubules in a 2D square domain of length L . Microtubules are shown in black, where the arrow represents the plus end. Also, microtubule orientation is measured from the horizontal of the minus end of the microtubule. Bound motors are red, and unbound motors are blue. (For interpretation of the references to color in this figure caption, the reader is referred to the web version of this paper.)

including a second pair of equations for a second bound/unbound motor pair in Section 3.2. In Section 3.2.1, we show how combinations of aster and vortex patterns form in systems comprised of both plus and minus-end directed motors, and in Section 3.2.2, we show how mitotic motor proteins (motors that have properties similar to motors found in the mitotic spindle) can form MTs into anti-parallel bundles. We conclude with a discussion in Section 4.

2. Modeling

In Section 2.1, we describe the model development; in Section 2.2, we describe the numerical details of simulations.

2.1. Model set-up

Our model, shown schematically in Fig. 2, describes the dynamic interactions between MTs and motors. Here, we consider a square domain Ω , where $\Omega = (0, L) \times (0, L)$, to represent a simplification of the cross-section through a cell. We denote the density of MT negative ends at time $t > 0$, location $\vec{x} \in \Omega$, and angle $\theta \in [-\pi, \pi]$, by $p(\vec{x}, t, \theta)$, where the orientation θ is measured from the horizontal of the minus end to the MT (as shown in Fig. 2). We assume that each motor is in one of two states, bound (shown in red in Fig. 2) or unbound (shown in blue in Fig. 2), and denote the density of each at location \vec{x} and time t by $m_b(\vec{x}, t)$ and $m_u(\vec{x}, t)$, respectively. The model equations are

$$\frac{\partial m_b(\vec{x}, t)}{\partial t} + \mathbf{v}_b \cdot \nabla_{\vec{x}} (m_b(\vec{x}, t)) = k_{on}(\tilde{p}) m_u(\vec{x}, t) - k_{off} m_b(\vec{x}, t), \quad (2.1)$$

$$\frac{\partial m_u(\vec{x}, t)}{\partial t} - D_u \Delta_{\vec{x}} m_u(\vec{x}, t) = -k_{on}(\tilde{p}) m_u(\vec{x}, t) + k_{off} m_b(\vec{x}, t), \quad (2.2)$$

$$\frac{\partial p(\vec{x}, t, \theta)}{\partial t} + S_{MT} \hat{\theta} \cdot \nabla_{\vec{x}} p(\vec{x}, t, \theta) = -\lambda(m_b) p(\vec{x}, t, \theta) + \lambda(m_b) \int_{-\pi}^{\pi} k(\theta, \tilde{\theta}, m_b) p(\vec{x}, t, \tilde{\theta}) d\tilde{\theta}. \quad (2.3)$$

Eq. (2.1) describes directed transport of motors along MTs and Eq. (2.2) describes the diffusion of unbound motors. Also, both Eqs. (2.1) and (2.2) have terms to describe switching between populations of bound and unbound motors. Eq. (2.3) describes treadmilling of MTs, as well as the alignment of MTs by their interactions with bound motors.

The right-hand side of Eqs. (2.1) and (2.2) state that bound motors detach from MTs at a rate k_{off} and that unbound motors become bound motors by attaching to MTs at a rate $k_{on}(\tilde{p})$. Here, the rate k_{off} is constant, whereas the rate $k_{on}(\tilde{p})$ depends on the total MT density $\tilde{p}(\vec{x}, t) = \int_{-\pi}^{\pi} p(\vec{x}, t, \theta) d\theta$ at each point in the domain and at each time. For simplicity, as well as for mathematical reasons (Hillen et al., 2014), we assume that k_{on} is a (bounded) first-order Hill function with respect to the total MT minus-end density \tilde{p} . That is,

$$k_{on}(\tilde{p}) = k_{on}^{max} \frac{\tilde{p}}{1 + \tilde{p}}, \quad (2.4)$$

where k_{on}^{max} is the maximum rate of attachment. For processive motors, k_{off} will be low and k_{on}^{max} will be high, and for non-processive motors the opposite will be true. Values of k_{off} and k_{on}^{max} for processive and non-processive motors are specified in Table 1.

The left-hand side of Eq. (2.1) states that motors move along MTs at a constant speed in the direction of the mean MT orientation. Here, we define the mean MT orientation vector at

Table 1
Model parameter values and sources for the full model.

| parameter | value | meaning | source |
|----------------------------------|----------------------------------|---|---------------------------|
| $\ \mathbf{v}_b\ _{ConvKinesin}$ | $0.8 \mu\text{ms}^{-1}$ | Speed of conventional kinesin <i>in vitro</i> | Howard, 2001 |
| $\ \mathbf{v}_b\ _{NCD}$ | $0.12 \mu\text{ms}^{-1}$ | Speed of NCD motor <i>in vitro</i> | Hentrich and Surrey, 2010 |
| $\ \mathbf{v}_b\ _{slow}$ | $0.04 \mu\text{ms}^{-1}$ | Max speed kinesin-5 <i>in vitro</i> | Hentrich and Surrey, 2010 |
| k_{on}^{max} high | 10 s^{-1} | Max attachment rate for processive motors | Surrey et al., 2001 |
| k_{on}^{max} low | 0.1 s^{-1} | Max attachment rate for non-processive motors | This paper |
| k_{off} low | 0.1 s^{-1} | Dissociation rate of processive motors | Surrey et al., 2001 |
| k_{off} high | 10 s^{-1} | Dissociation rate of non-processive motors | This paper |
| D_u | $0.2 \mu\text{m}^2\text{s}^{-1}$ | Diffusion constant for motors | This paper |
| S_{MT} high | $0.12 \mu\text{ms}^{-1}$ | Treadmilling speed of interphase MTs released from the centrosome of fibroblastic cells <i>in vitro</i> | Rodionov et al., 1999 |
| S_{MT} low | $0.04 \mu\text{ms}^{-1}$ | Typical treadmilling speed of MTs grown <i>in vitro</i> | Rodionov et al., 1999 |
| λ_{max} | 40 s^{-1} | Switching rate of MTs | This paper |
| C low | 0.1 | Motor activity parameter | This paper |
| C high | 25 | Motor activity parameter | This paper |

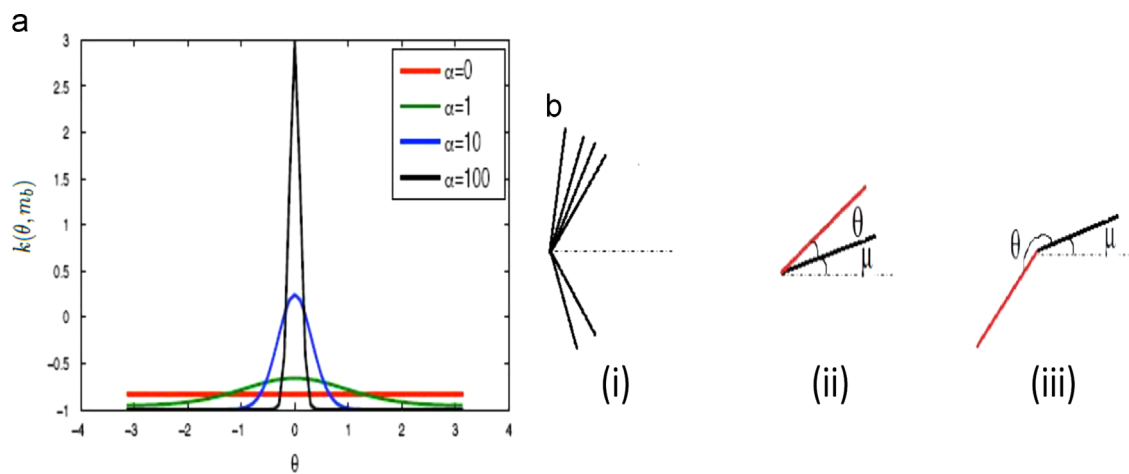


Fig. 3. (a) MT redistribution kernel k (Eq. (2.10)) centered at mean $\mu=0$ for different values of α . (b) (i) A group of MTs with different orientations whose minus ends are centered at the same point. (ii) The mean orientation of MTs μ in (i) is shown in black and a possible angle of reorientation θ is shown in red. (iii) The mean orientation of MTs μ in (i) is shown in black and a second possible angle of reorientation θ is shown in red. It is more likely for MTs to be reoriented to the angle θ in (ii) (rather than the angle θ in (iii)), as a result of the assumptions we make. (For interpretation of the references to color in this figure caption, the reader is referred to the web version of this paper.)

each point in space by $\hat{\mu} = (\mu_x, \mu_y)$, where the horizontal and vertical components μ_x and μ_y are given by Eqs. (2.5) and (2.6), respectively, and describe the integral mean of the x and y components of the MT orientation, where $x = \cos(\theta)$ and $y = \sin(\theta)$.

$$\mu_x = \frac{\int_{-\pi}^{\pi} \cos(\theta) p(\vec{x}, t, \theta) d\theta}{\int_{-\pi}^{\pi} p(\vec{x}, t, \theta) d\theta} \quad (2.5)$$

$$\mu_y = \frac{\int_{-\pi}^{\pi} \sin(\theta) p(\vec{x}, t, \theta) d\theta}{\int_{-\pi}^{\pi} p(\vec{x}, t, \theta) d\theta} \quad (2.6)$$

The mean angle μ (written as a scalar value) is given by

$$\mu = \arctan(\mu_x/\mu_y) + j\pi, \quad (2.7)$$

where $j=0$ if $\mu_x > 0$, $j = -1$ if $\mu_x < 0$ and $\mu_y < 0$, and $j=1$ if $\mu_x < 0$ and $\mu_y > 0$.

It has been found that motor protein speed depends on whether the motor protein is carrying a light or heavy load (the lighter the load, the faster the motor) (Howard, 2001). Also, it has been found that motor speed may depend on the number of motors present (the more motors present, the slower the speed). However, in this paper we will neglect load mass and motor

density and write the velocity \mathbf{v}_b in the following way,

$$\mathbf{v}_b = -\|\mathbf{v}_b\| \hat{\mu} = -\|\mathbf{v}_b\| \begin{pmatrix} \mu_x \\ \mu_y \end{pmatrix}. \quad (2.8)$$

Here, the speed $\|\mathbf{v}_b\|$ is constant, and the negative sign accounts for the fact that we are considering minus-end directed motors (like kinesin-14), where such motors move in a direction that is opposite to the mean MT orientation vector $\hat{\mu}$ (a unit vector). If we are considering plus-end directed motors (like kinesin-1), we change this sign to positive.

The second equation for motor movement, Eq. (2.2) states that unbound motors diffuse freely in the absence of MTs with diffusion constant D_u . In the presence of MTs, we have similar switching terms as the bound motors in Eq. (2.1). That is, unbound motors attach to MTs at rate $k_{on}(\hat{p})$ and bound motors become unbound motors at rate k_{off} .

Finally, the equation for MT movement given by Eq. (2.3) describes the time evolution of MTs due to the fact that MTs can move in a directed path by treadmilling and can realign due to their interactions with moving motors. The expression on the left side of Eq. (2.3) accounts for directed MT motion along the axis of the MT $\hat{\theta}$ with constant speed S_{MT} , where $\hat{\theta} = \begin{pmatrix} \cos(\theta) \\ \sin(\theta) \end{pmatrix}$.

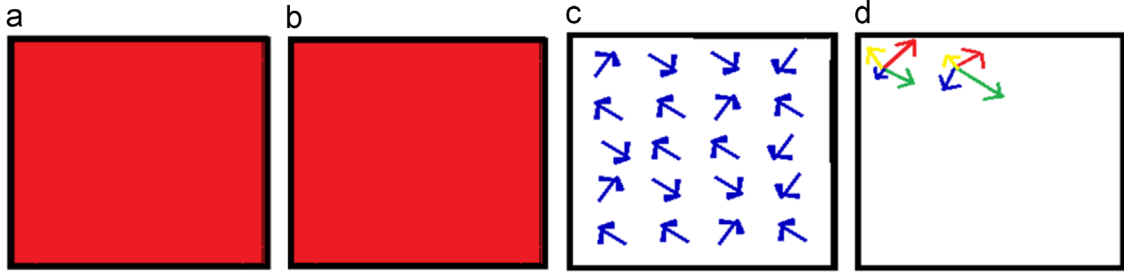


Fig. 4. The initial conditions for the model. (a) Motor density is fixed and uniform in space. (b) MT density is initially uniform. Red represents high density. (c) A schematic of the mean MT orientation μ at each point in space. (d) A schematic of the full MT orientation distribution at two points in space (only four possible orientations and two spatial locations are shown for clarity). (For interpretation of the references to color in this figure caption, the reader is referred to the web version of this paper.)

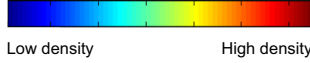


Fig. 5. MT density color bar. In this and all subsequent figures, colors vary from low MT density (blue) to high MT density (red). (For interpretation of the references to color in this figure caption, the reader is referred to the web version of this paper.)

The last terms on the right-hand side of Eq. (2.3) represent non-local interactions between MTs. In particular, it is the stochastic part of the model and describes a velocity jump process for MT reorientation (Othmer, 2010; Othmer et al., 1988). Such processes are commonly used to describe systems that exhibit a sequence of ‘runs’ (directed motion) separated by reorientations. At any instance, the MT can change its orientation when in the presence of motor proteins, and does so at the rate $\lambda(m_b)$. We choose $\lambda(m_b)$ to be a Hill function with respect to the bound motor density m_b . That is,

$$\lambda(m_b) = \lambda_{\max} \frac{m_b}{1 + m_b}, \quad (2.9)$$

where λ_{\max} is the maximum switching rate. We choose this type of function since we expect the switching rate to saturate at a maximum value. The term $k(\theta, \tilde{\theta}, m_b)$ is a probability density function describing a reorientation of a MT from the angle $\tilde{\theta}$ to θ (and depends on m_b). We choose k to be a Von Mises distribution (Othmer et al., 1988; Johnson and Kotz, 1970)

$$k(\theta, \tilde{\theta}, m_b) = \frac{1}{2\pi I_0(\alpha(m_b))} \exp(\alpha(m_b) \cos(\theta - \mu)), \quad (2.10)$$

where $I_0(\alpha(m_b))$ is a modified Bessel function of order 0 with parameter $\alpha(m_b)$, and μ and $1/\alpha(m_b)$ are the mean and variance of the distribution, respectively. Fig. 3(a) illustrates k centered at mean $\mu = 0$ for various values of the variance $1/\alpha(m_b)$.

In the limits of α going to zero and infinity, we get

$$\lim_{\alpha \rightarrow 0} p(\theta) = \frac{1}{2\pi}, \quad (2.11)$$

$$\lim_{\alpha \rightarrow \infty} p(\theta) = \delta(\mu), \quad (2.12)$$

where $\delta(\mu)$ is the dirac delta functional and can be defined (loosely) by

$$\delta(\theta) = \begin{cases} \infty & \text{if } \theta = \mu \\ 0 & \text{if } \theta \neq \mu. \end{cases}$$

Our choice of k implies that the probability of recruitment of a MT at a point \vec{x} to an angle θ depends only on how close that angle is to the mean MT orientation μ (described in Eq. (2.7)). In particular, the probability of recruitment does not depend on the angle from which the MT came, namely $\tilde{\theta}$. This assumption not only allows the model to be analyzed more easily, since k can be pulled outside of the integral term in Eq. (2.3) (as explained in

Hillen et al. (2014)), but it is also biologically realistic. In Fig. 3(b), we describe how, at every time step, and at every location \vec{x} , the MT network tends to align towards its mean μ .

Since we have assumed that MTs tend to align to the mean MT orientation μ in the presence of bound motors m_b (and that there is no alignment when there are no motors present), we choose $\alpha(m_b)$ to be some monotonically increasing function of m_b , so that when many bound motors are present, the distribution is concentrated about the mean μ , and alignment is more likely. Also, if m_b is very small, the distribution is close to uniform, and alignment is less likely. We call $\alpha(m_b)$ the alignment function, and can choose it to be any monotonically increasing function with respect to m_b . For simplicity we choose $\alpha(m_b)$ to be a linear function with respect to m_b so that,

$$\alpha(m_b) = C m_b, \quad (2.13)$$

where we call C the *motor activity parameter*. For a fixed value of m_b , alignment is more likely for large values of C . That is, motors with larger values of C are more effective cross-linkers. Similarly, for a fixed value of C , alignment is more likely for large values of m_b . Table 1 is a summary of model parameters used in this paper.

2.2. Boundary conditions and numerical scheme

For simplicity in reading, we write $p(\vec{x}, t, \theta) = p(x, y, t, \theta)$, where $\vec{x} = (x, y)$, and consider only periodic boundary conditions,

$$\begin{aligned} m_b(0, y, t) &= m_b(L, y, t), \\ m_u(0, y, t) &= m_u(L, y, t), \\ p(0, y, t, \theta) &= p(L, y, t, \theta); p(x, 0, t, \theta) = p(x, L, t, \theta). \end{aligned} \quad (2.14)$$

Periodic boundary conditions are appropriate because the experiments to which we compare our simulation results are conducted on large domains (Surrey et al., 2001) where boundary effects are negligible.

To simulate the advection parts of the model (the left-hand side of Eqs. (2.1) and (2.3)), we use a first-order upwind scheme at each location. The direction of the upwind velocity depends on the MT direction θ . For example, if $\theta = 3\pi/4$, the direction vector $\hat{\theta} = \begin{pmatrix} \cos(\theta) \\ \sin(\theta) \end{pmatrix} = \begin{pmatrix} -0.7071 \\ 0.7071 \end{pmatrix}$, and we perform upwinding in the negative x direction and upwinding in the positive y direction. To simulate the diffusion part of Eq. (2.2) we use an explicit central difference scheme. By using such a scheme, we are restricted to studying motors with slow diffusion rates. In future studies, we will test more realistic, faster diffusion rates, perhaps by developing an implicit-type diffusion scheme.

To simulate the integral term on the right-hand side of Eq. (2.3), we use the Trapezoid Rule. All simulations are implemented in Matlab using custom code, using a 60×60 unit spatial grid (each unit $\simeq 1.0 \mu\text{m}$, so we are looking at a medium sized cell of size $60 \times 60 \mu\text{m}^2$) and an angular grid between $-\pi$ and π with a step size of $\pi/32$. Simulations on smaller angular grids show similar results.

Fig. 4 describes the motor distribution and the initial conditions for MTs. Fig. 4(a) describes the initial motor distribution. Fig. 4(b) illustrates the initial MT density, which is chosen to be uniform throughout the entire domain ($\approx 0.1 \mu\text{m}^{-2}$), Fig. 4(c) illustrates the initial mean MT orientation at each spatial location, and Fig. 4(d) illustrates the orientational distribution at each spatial location (each MT is assigned a random orientation between $-\pi$ and π). Each color represents a different orientation, and the length of the vector is proportional to the density of MTs oriented along that direction. To keep the schematic less clustered, we only show four possible orientations, and 20 spatial locations. However, for our simulations, we allow a total of 64 possible orientations for MTs at each spatial location. Fig. 5 illustrates MT density, where high MT density corresponds to red and low MT density corresponds to blue (initially, MTs are uniform everywhere in space so the color is red everywhere, as shown in Fig. 4(b)).

3. Results of numerical simulations

In this section, we describe numerical results for the full model given by Eqs. (2.1), (2.2) and (2.3) using periodic boundary conditions. We describe MT patterns that are observed from the simulation of these equations using parameter values that are representative of motor proteins used in *in vitro* experiments (Nedélec et al., 1997; Surrey et al., 2001). The parameters specific to motors are bound motor speed $\|\mathbf{v}_b\|$, the max attachment rate k_{on}^{max} , and the detachment rate k_{off} . Values for these parameters are found in Table 1.

For MT dynamics, we choose the maximum switching rate λ_{max} to be the same in every simulation, the treadmilling speed S_{MT} to be low (unless stated otherwise), and the motor activity C to be low (values found in Table 1). The reason we choose a low value for C is that we describe MT patterns formed for various values of the motor density (low, moderate, and high), and since the alignment function $\alpha(m_b)$ depends directly on both C and m_b (alignment function given by Eq. (2.13)), an increase in m_b has a similar effect as an increase in C . Also, when we describe patterns as being at steady-state, this means that patterns are stable and do not change with time (verified by the inspection of images after long-time simulation n).

In Section 3.1, we show results for simulation of MT/motor systems comprised of a single processive motor type, and in Section 3.2, we show results for MT/motor systems comprised of two opposing motor types. In all Figs. 6–12 (except the motor protein plots shown in Figs. 10 and 12), the first plot (a) corresponds to the MT density in the (x, y) plane, the second plot (b) corresponds to the mean MT orientation at each spatial point in the (x, y) plane, and the third plot (c) corresponds to an enlargement of (b) over a small portion of the domain.

3.1. MT patterning in the presence of one motor type

In this section, we investigate MT patterning under the influence of one processive motor type, where the maximum attachment rate k_{on}^{max} is high and the detachment rate k_{off} is low. We consider NCD-type motors (where the bound motor speed $\|\mathbf{v}_b\|$ is high and negative), or conventional kinesin-type motors (where the bound motor speed $\|\mathbf{v}_b\|$ is very high and positive).

Fig. 6 shows steady-state results for a low density of NCD-type motors. We find that for low motor density and low MT treadmilling speed S_{MT} , MTs form stable, minus-end focused asters at steady state, where motors (bound and unbound) are located at the center of the asters (motor results not shown). If we increase motor density to moderate and high values, 0.1 and $1.0 \mu\text{m}^2$, respectively, the asters persist. However, the number of asters

increases as we increase motor density. We considered high MT treadmilling speeds S_{MT} , and results were similar: motors are able to focus MTs into minus-end focused asters (results not shown).

For plus-end directed kinesin-type motors, we find that plus-end focused asters form at low and high motor densities (results not shown). However, if we double the MT treadmilling speed S_{MT} , vortices form at low motor densities, as shown in Fig. 7. We define vortex formation as rotation about a point (i.e., rotation can be circular or ellipsoidal, and can be directed in or out). For higher motor density, asters form instead of vortices, similar to the case where we have low MT treadmilling speed. Similar to NCD motors, both bound and unbound motors are located at the centers of each aster or vortex (results not shown).

3.2. MT patterning in the presence of two opposing motor types

In this section, we investigate MT patterning under the influence of two types of motors with opposing directionality. In this case, the model given by Eqs. (2.1) and (2.3) includes two more equations, similar to Eqs. (2.1) and (2.2), for the second class of motor protein considered. The only change to this class of motors is a change in sign in front of the advection term for bound motors in Eq. (2.1). In Section 3.2.1, we choose motor parameter values similar to those used in the previous Section 3.1. In Section 3.2.2, we show results for systems comprised of two opposing motor types that are found in the mitotic spindle during cell division (Wordeman, 2010).

3.2.1. Two processive motors

Here, we consider a system consisting of the two processive motors used in the previous section (similar to the motors used in Surrey et al. (2001)). That is, we consider the moderately fast, processive, minus-end directed NCD motors and the faster, processive, plus-end directed conventional kinesin motors.

First, we consider the case where the MT treadmilling speed is low. As shown in Section 3.1, both plus- and minus-end directed motors alone focus MTs into asters at all motor densities when the treadmilling speed is low. Fig. 8 shows results for low (and equal) motor density, and low treadmilling speed for MTs when both motor types are present. We obtain a mixture of plus-end focused and minus-end focused asters. We find that the asters are very tight (small and isolated from one another) and so they are very difficult to see, unless we enlarge a small portion of the domain (as in Fig. 8(c)). As we increase motor density, the number of asters increases, making it increasingly difficult to distinguish one aster from another. Kinesin motors are located at the center of plus-end focused asters and NCD motors are located at the center of minus-end directed asters (results not shown).

As a second example, we consider the case where MT treadmilling speed is high. In this situation, previous simulations from Section 3.1 show that conventional kinesin motors alone will form vortices at low motor density and asters at higher motor densities, while NCD motors form asters at all motor densities. Here, we select a low (and equal) motor density for each motor type to test whether systems comprised of vortices and asters exist. In Fig. 9, we show results when both motor types are present and treadmilling speed is high. We find mixtures of vortices (formed by kinesin motors) and asters (formed by NCD motors). Fig. 10 shows that kinesin motors (bound and unbound) are found at the center of vortices, while NCD motors (bound and unbound) are found at the center of minus-focused asters.

3.2.2. Example of two opposing motors found in the mitotic spindle

In this section, we test what patterns can be observed in the presence of two opposing motor types with properties that are

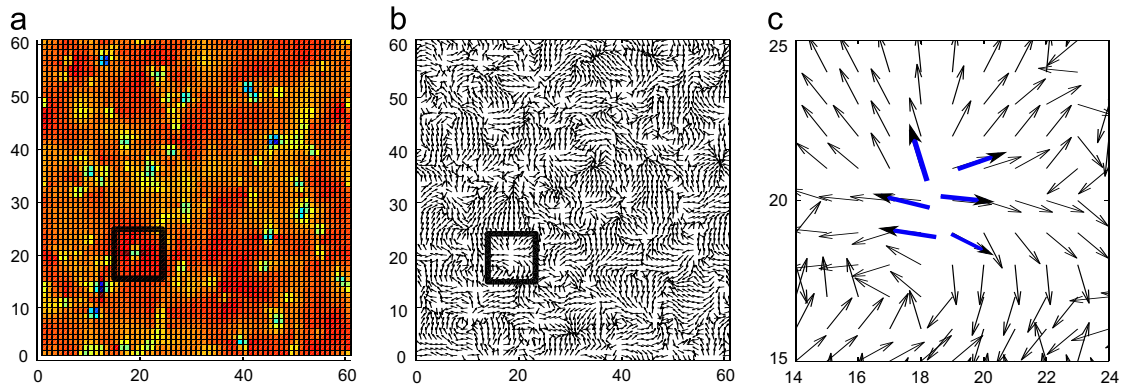


Fig. 6. Steady-state minus-end focused asters for NCD-type motors at moderate motor density and low treadmilling speed. Here, $k_{\text{on}}^{\text{max}} = 10/s$, $k_{\text{off}} = 0.1/s$, and $\|\mathbf{v}_b\| = 0.12 \mu\text{m}/s$ and total motor density is moderate ($0.1 \mu\text{m}^{-2}$). (a) MT density; (b) MT orientation; (c) Region of MT orientation plot enlarged to show a single aster on a small patch of the domain. Blue arrows highlight a minus-end focused aster. (For interpretation of the references to color in this figure caption, the reader is referred to the web version of this paper.)

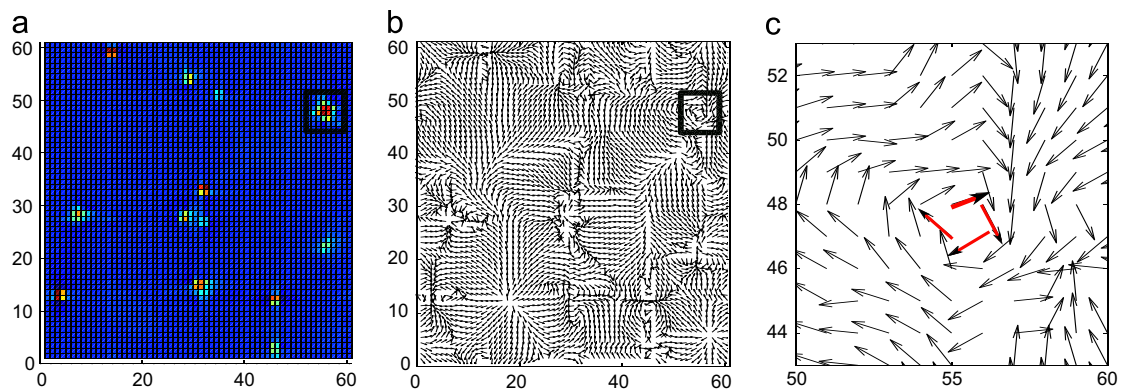


Fig. 7. Steady-state vortices for plus-end directed conventional kinesin-type motors at low motor density and high treadmilling speed. Here, $k_{\text{on}}^{\text{max}} = 10/s$, $k_{\text{off}} = 0.1/s$, and $\|\mathbf{v}_b\| = 0.8 \mu\text{m}/s$ and total motor density is low ($0.05 \mu\text{m}^{-2}$). (a) MT density; (b) MT orientation; (c) Region of MT orientation plot enlarged to show a single vortex on a small patch of the domain. Red arrows highlight a vortex. (For interpretation of the references to color in this figure caption, the reader is referred to the web version of this paper.)

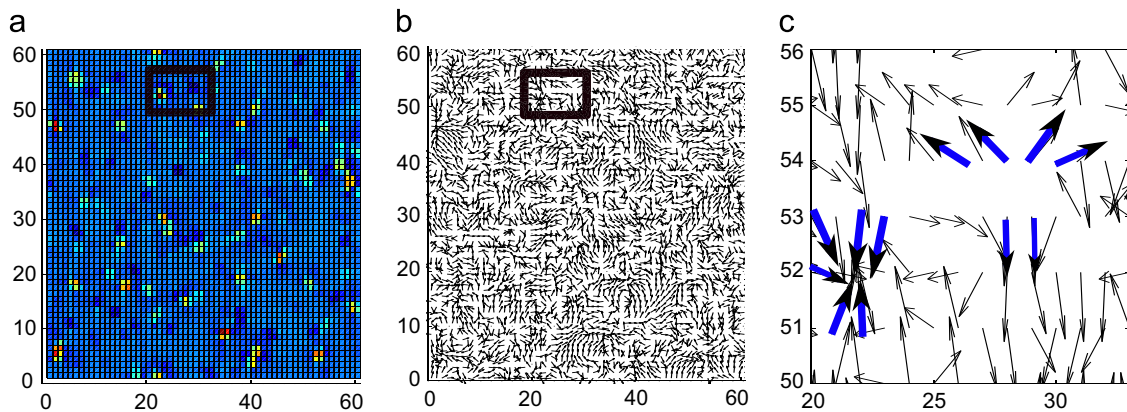


Fig. 8. A mixture of plus-end focused asters and minus-end focused asters forms in systems of NCD and conventional kinesin when the treadmilling speed is low. Here, $k_{\text{on}}^{\text{max}} = 10/s$, $k_{\text{off}} = 0.1/s$ for both motors, $\|\mathbf{v}_b\| = 0.12 \mu\text{m}/s$ for NCD, and $\|\mathbf{v}_b\| = 0.8 \mu\text{m}/s$ for kinesin, and the motor density is low ($0.05 \mu\text{m}^{-2}$). (a) MT density; (b) MT orientation; (c) Region of MT orientation plot enlarged to show a plus and minus-focused aster on a small patch of the domain. Blue arrows highlight two asters. (For interpretation of the references to color in this figure caption, the reader is referred to the web version of this paper.)

similar to those found in the mitotic spindle (Wordeman, 2010). In particular, we use parameters for the minus-end directed motor, kinesin-14, and the plus-end directed motor, kinesin-5. Kinesin-5 is sometimes found to be processive, while at other times it is weakly processive. Here, we choose the motor to be processive and the speed to be its *in vitro* speed (as recorded in Table 1). Kinesin-14, also referred to as mitotic NCD, is non-processive in the mitotic spindle. Thus, it is different from the processive NCD construct used in the previous section. In particular, for the

following simulations of kinesin-14, we use values for k_{off} and $k_{\text{on}}^{\text{max}}$ that correspond to a very weak/non-processive motor (Table 1). Fig. 11 shows the results for MT density and orientation when both kinesin-14 and kinesin-5 are present and Fig. 12 shows results for the densities of both bound and unbound motors. Fig. 11 shows large patches where anti-parallel MT bundles form in the presence of kinesin-14 and kinesin-5 at equal (and low) densities. Also, Fig. 12 shows that plus-end kinesin-5 motors are located in a string-like pattern corresponding to the locations of the plus ends

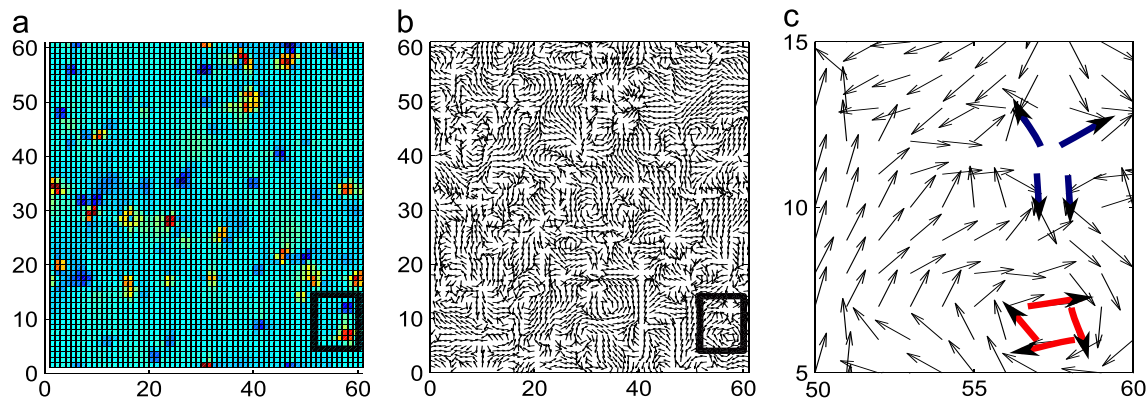


Fig. 9. A mixture of vortices and asters forms in systems of NCD and conventional kinesin when treadmilling speed is high. Here, $k_{on}^{max} = 10/s$, $k_{off} = 0.1/s$ for both motors, $\|\mathbf{v}_b\| = 0.8\mu\text{m/s}$ for kinesin, $\|\mathbf{v}_b\| = 0.12\mu\text{m/s}$ for NCD, and motor density for each motor is low ($0.05\mu\text{m}^{-2}$). (a) MT density; (b) MT orientation; (c) Region of MT orientation plot enlarged to show a single aster and a single vortex on a small patch of the domain. Red arrows highlight a vortex and blue arrows highlight an aster.

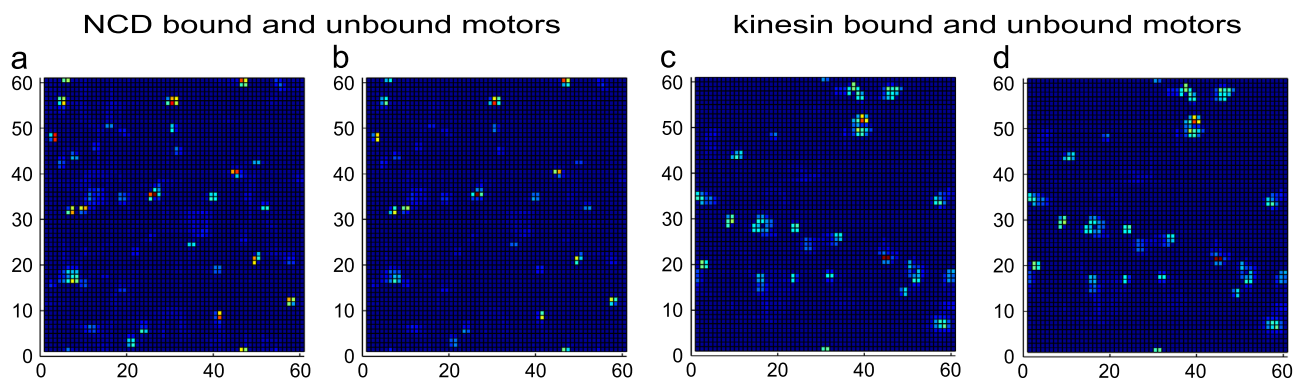


Fig. 10. Location of bound and unbound motors for (a, b) NCD motors, and (c, d) kinesin motors from the simulation shown in Fig. 9.

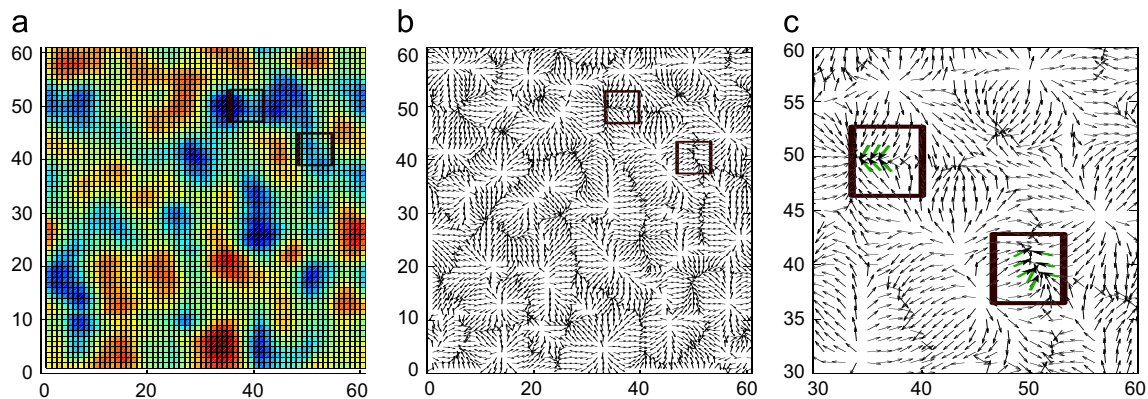


Fig. 11. Anti-parallel bundles form in systems of kinesin-14 (mitotic NCD) and kinesin-5 when treadmilling speed is low. Here, $k_{on}^{max} = 0.1/s$ and $k_{off} = 10/s$ for kinesin-14, and $k_{on}^{max} = 10/s$, $k_{off} = 0.1/s$ for kinesin-5. $\|\mathbf{v}_b\| = 0.12\mu\text{m/s}$ for kinesin-14, $\|\mathbf{v}_b\| = 0.04\mu\text{m/s}$ for kinesin-5, and motor density for each motor is low ($0.01\mu\text{m}^{-2}$). (a) MT density; (b) MT orientation; (c) Region of MT orientation plot enlarged to show anti-parallel bundling on a small patch of the domain. Green arrows highlight a string of anti-parallel MTs. (For interpretation of the references to color in this figure caption, the reader is referred to the web version of this paper.)

of the MTs. Minus-end directed kinesin-14 motors are more evenly dispersed, but are not located in regions where plus-end directed kinesin-5 motors are located.

4. Discussion

In this paper, we have developed a model to represent the dynamic interaction between mobile motor proteins and MTs. In particular, we describe interactions of MTs with two motor constructs, processive kinesin and processive NCD, also used in the *in vitro* experiments of Surrey et al., 2001. We also simulate our

model using properties specific to mitotic motors to obtain anti-parallel bundle patterns that are found *in vivo*.

For NCD-type motors, we find that MTs form stable minus-end focused asters with motors located at aster centers. This is true for low to high motor densities and for low to high MT treadmilling speeds. These results are consistent with experimental results found by Surrey et al. (2001), who showed that MTs form minus-end focused asters for low and high NCD motor densities.

For plus-end directed kinesin-type motors, we find that vortices can form at low motor densities and for high MT treadmilling speeds, where motors are located at the vortex centers. At higher

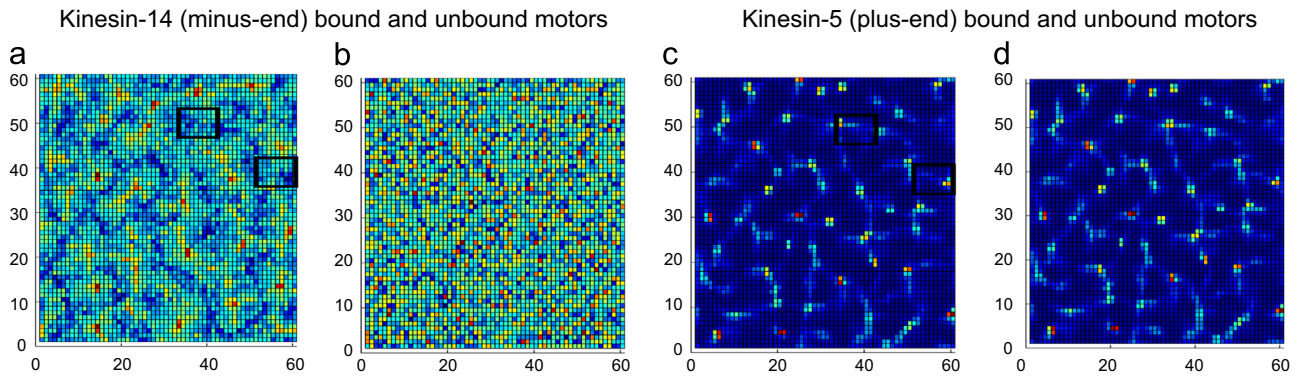


Fig. 12. Location of bound and unbound motors for (a, b) kinesin-14 (mitotic NCD) motors, and (c, d) Kinesin-5 motors from the simulation shown in Fig. 11.

densities (and lower MT treadmilling speeds) such vortices do not form, but plus-end focused asters form instead, consistent with Surrey et al. (2001).

In systems comprised of both motor types described above, results show that either systems of asters and vortices form, or systems of only asters form (minus and plus-end focused asters). Similar results are discussed in Surrey et al. (2001).

Finally, for systems with mitotic kinesin-14 and kinesin-5 motors, simulation results show that large string-like bundles of anti-parallel MTs form, where MT plus ends meet at the anti-parallel bundle midzone. This result is consistent with patterning observed during mitosis *in vivo*. That is, MTs form anti-parallel bundles (the mitotic spindle) during cell division, and MT plus ends are located at the midzone of the anti-parallel bundles (Karp, 1996). While many other components are involved in forming the mitotic spindle *in vivo*, the model results suggest that two opposing mitotic motors may play a critical role in forming this structure. Indeed, *in vitro* studies by Mitchison et al. have found that, in systems where MTs stabilized by taxol (Zhou and Giannakakou, 2005) are mixed with the mitotic motors dynein and kinesin-5, as well as other mitotic proteins such as Aurora B and Kif4, MTs are able to slowly stabilize into patterns of anti-parallel bundled lines or open circles (referred to as pineapples). In both our simulations and the experiment of Mitchison et al. (2013), the bundled lines are ordered so that the plus ends of the MTs meet in the midzone of each line.

It should be noted that, for the resulting patterns to form, the model requires an advection-type term. Here, we assume treadmilling is the mechanism for directed transport. Alternatively, we could describe directed transport of MTs using a sliding mechanism, as investigated by us in White et al. (2014) (sliding under the influence of stationary motors), as well as by Aranson and Tsimring (2006) (sliding under the influence of moving motors). Unlike treadmilling, for sliding, translocation may be directed to either the plus-end direction of a MT (under the influence of minus-end directed motors), or towards the minus-end direction (for plus-end directed motors). Also, different from treadmilling, sliding occurs only in the presence of motors, and so translocation due to sliding would depend on motor density. It would be interesting to incorporate such a mechanism into our model in future investigations.

In conclusion, by simulating a mathematical model for MT evolution in the presence of moving motor proteins, we have found MT patterns similar to those found *in vitro* and *in vivo*. In particular, we have found that MT patterns such as vortices, asters, and anti-parallel bundles can form in the presence of different types of motor proteins, where such patterns depend on the particular properties of such motor proteins. Our results are

consistent with experimental data that suggest MT patterning depends on motor speed, directionality, processivity, and concentration, as well as MT treadmilling and MT alignment caused by interactions with motors. Our model was also expanded to include dynamic interactions of MTs with two motor types (and not just one type as in previous models). In doing this, we were able to describe anti-parallel bundling, something that has not been done with previous models.

References

- Aranson, I., Tsimring, L., 2006. Theory of self-assembly of microtubules and motors. *Phys. Rev. E* 74, doi: 031915.
- Cytrynbaum, E., Rodionov, V., Mogilner, A., 2006. Nonlocal mechanism of self-organization and centering of microtubule asters. *Bull. Math. Biol.* 68, 1053–1072.
- Dogterom, M., Surrey, T., 2013. Microtubule organization *in vitro*. *Curr. Opin. Cell Biol.* 25, 23–29.
- Gibbons, F., Chauwin, J.-F., Despósito, M., José, J., 2001. A dynamical model of kinesin-microtubule motility assays. *Biophys. J.* 80, 2515–2526.
- Hentrich, C., Surrey, T., 2010. Microtubule organization by the antagonistic mitotic motors kinesin-5 and kinesin-14. *J. Cell Biol.* 189 (3), 465–480.
- Hillen, T., White, D., de Vries, G., Dawes, A., 2015. Existence and uniqueness for a coupled pde model for motor induced microtubule organization, submitted to SIAP.
- Hillen, T., 2006. M5 mesoscopic and macroscopic models for mesenchymal motion. *J. Math. Biol.* 53, 585–615.
- Howard, J., 2001. *Mechanics of Motor Proteins and the Cytoskeleton*. Sinauer Associates, Sunderland.
- Jia, Z., Karpeev, D., Aranson, I., Bates, P., 2008. Simulation studies of self-organization of microtubules and molecular motors. *Phys. Rev. E* 77, doi: 051905.
- Johnson, N., Kotz, L., 1970. *Distributions in Statistics—Continuous Univariate Distributions*, second ed. John Wiley and Sons, New York.
- Karp, G., 1996. *Cell and Molecular Biology*. John Wiley and Sons, New York.
- Kim, J., Park, Y., Kahng, B., Lee, H.Y., 2003. Self-organized patterns in mixtures of microtubules and motor proteins. *J. Korean Phys. Soc.* 42 (1), 162–166.
- Kirschner, M., Mitchison, K., 1984. Dynamic instability of microtubule growth. *Nature* 312, 237–242.
- Lee, H.Y., Kardar, M., 2001. Macroscopic equations for pattern formation in mixtures of microtubules and molecular motors. *Am. Phys. Soc.* 64, doi: 056113.
- Ma, R., Laan, L., Dogterom, M., Pavin, N., Jülicher, F., 2014. General theory for the mechanics of confined microtubule asters. *New J. Phys.* 16, doi: 10.1088.
- Mitchison, K., Kirschner, M., 1986. Beyond self-assembly: from microtubules to morphogenesis. *Cell* 45, 329–342.
- Mitchison, T., Nguyen, P., Coughlin, M., Groen, A., 2013. Self-organization of stabilized microtubules by both spindle and midzone mechanisms in *Xenopus* egg cytosol. *Mol. Biol. Cell* 24, 1559–1573.
- Nedélc, F., Surrey, T., 2001. Dynamics of microtubule aster formation by motor complexes. *Phys. Scale Cell* 4, 841–847.
- Nedélc, F., Surrey, T., Maggs, A.C., Leibler, S., 1997. Self-organization of microtubules and motors. *Nature* 389, 305–308.
- Othmer, H., Dunbar, S., Alt, W., 1988. Models of dispersal in biological systems. *J. Math. Biol.* 26, 263–298.
- Othmer, H., 2010. Notes on space- and velocity-jump models of biological movement. *Theor. Biol.* 10, 913–917.
- Rodionov, V., Nadezhkina, E., Borisov, G., 1999. Centrosomal control of microtubule dynamics. In: *Proceedings of the National Academy of Science*, vol. 96, pp. 115–120.

- Surrey, T., Nedélec, F., Leibler, S., Karsenti, E., 2001. Physical properties determining self-organization of motors and microtubules. *Science* 292, 1167–1171.
- Tao, L., Mogliner, A., Civelekoglu-Scholey, G., Wollman, R., Evans, J., Stahlberg, H., Scholey, J., 2006. A homotetrameric kinesin-5, klp61f, bundles microtubules and antagonizes ncd in motility assays. *Curr. Biol.* 16, 2293–2302.
- Vale, R., Malik, F., Brown, D., 1992. Directional instability of microtubule transport in the presence of kinesin and dynein, two opposite polarity motor proteins. *J. Cell Biol.* 119, 1589–1596.
- Wade, R., 2009. On and around microtubules: an overview. *Mol. Biotechnol.* 43, 177–191.
- Waterman-Storer, C., Salmon, E., 1997. Microtubule dynamics: treadmilling comes around again. *Curr. Biol.* 7, 369–372.
- White, D., de Vries, G., Dawes, A., 2014. Microtubule patterning in the presence of stationary motor distributions. *Bull. Math. Biol.* 76 (8), 1917–1940.
- Wordeman, L., 2010. How kinesin motor proteins drive mitotic spindle function: lessons from molecular assays. *Semin. Cell Dev. Biol.* 21, 260–268.
- Yokota, E., Sonobe, S., Igarashi, H., Shimmen, T., 1995. Plant microtubules can be traslocated by a dynein atpase from sea urchin in vitro. *Plant Cell Physiol.* 36 (8), 1563–1569.
- Zhou, J., Giannakakou, P., 2005. Targeting microtubules for cancer chemotherapy. *Curr. Med. Chem.* 5, 65–71.